Water Research 117 (2017) 175–186

Contents lists available at ScienceDirect

Water Research

journal homepage: www.elsevier.com/locate/watres

Treatment of arsenic in acid wastewater and river sediment by $Fe@Fe_2O_3$ nanobunches: The effect of environmental conditions and reaction mechanism

Lin Tang [a, b, *], Haopeng Feng [a, b], Jing Tang [a, b], Guangming Zeng [a, b, **], Yaocheng Deng [a, b], Jiajia Wang [a, b], Yani Liu [a, b], Yaoyu Zhou [c]

[a] College of Environmental Science and Engineering, Hunan University, Changsha, 410082, China
[b] Key Laboratory of Environmental Biology and Pollution Control (Hunan University), Ministry of Education, Changsha, 410082, China
[c] College of Resources and Environment, Hunan Agricultural University, Changsha, 410128, China

ARTICLE INFO

Article history:
Received 7 January 2017
Received in revised form
16 March 2017
Accepted 28 March 2017
Available online 31 March 2017

Keywords:
Arsenic treatment
Zero valent iron
Core-shell structure
$Fe@Fe_2O_3$ nanobunches
Adsorption
Oxidation

ABSTRACT

High concentration of arsenic in acid wastewater and polluted river sediment caused by metallurgical industry has presented a great environmental challenge for decades. Nanoscale zero valent iron (nZVI) can detoxify arsenic-bearing wastewater and groundwater, but the low adsorption capacity and rapid passivation restrict its large-scale application. This study proposed a highly efficient arsenic treatment nanotechnology, using the core-shell $Fe@Fe_2O_3$ nanobunches (NBZI) for removal of arsenic in acid wastewater with cyclic stability and transformation of arsenic speciation in sediment. The adsorption capacity of As(III) by NBZI was 60 times as high as that of nanoscale zero valent iron (nZVI) at neutral pH. Characterization of the prepared materials after reaction revealed that the contents of As(III) and As(V) were 65% and 35% under aerobic conditions, respectively, which is the evidence of oxidation included in the reaction process apart from adsorption and co-precipitation. The presence of oxygen was proved to improve the adsorption ability of the prepared NBZI towards As(III) with the removal efficiency increasing from 68% to 92%. In order to further enhance the performance of NBZI-2 in the absence of oxygen, a new Fenton-Like system of $NBZI/H_2O_2$ to remove arsenic under the anoxic condition was also proposed. Furthermore, the removal efficiency of arsenic in acid wastewater remained to be 78% after 9 times of cycling. Meanwhile, most of the mobile fraction of arsenic in river sediment was transformed into residues after NBZI treatment for 20 days. The reaction mechanism between NBZI and arsenic was discussed in detail at last, indicating great potential of NBZI for the treatment of arsenic in wastewater and sediment.

1. Introduction

Arsenic is one of the major environmental pollutants with a wide variety of detrimental effects on animals and humans, especially As(III). It may lead to tumorigenesis and chromosomal aberrations due to its long stay in human bodies (Neumann et al., 2013; Vadahanambi et al., 2013). Besides, The World Health Organization (WHO) has set a new guideline limit of arsenic (0.05–0.01 $\mu g\ L^{-1}$) in drinking water (Guan et al., 2012). For decades, large amount of sewage containing high concentration of arsenic has been generated in non-ferrous metal smelting process, especially in the smelting section and the flue gas acid washing recovery section, which is mainly acidic wastewater, causing great harm to the aqueous environment if not treated properly. Recently, the river sediment with arsenic pollution has attracted widespread attention owing to its high toxicity, and even at a low concentration it can cause tremendous harm to living organisms (De Jonge et al., 2012). Shimen realgar mine is situated in Dieshui River basin, Hunan Province in China which used to be the largest realgar mine in Asia. The mine was exploited for 1500 years for production of sulfuric acid and arsenic used in the manufacture of firecrackers, medicinal realgar (As_4S_4). The boosting exploitation and improper treatment

* Corresponding author. College of Environmental Science and Engineering, Hunan University, Changsha, 410082, China.
** Corresponding author. College of Environmental Science and Engineering, Hunan University, Changsha, 410082, China.
E-mail addresses: tanglin@hnu.edu.cn (L. Tang), zgming@hnu.edu.cn (G. Zeng).

http://dx.doi.org/10.1016/j.watres.2017.03.059
0043-1354/

of mining and smelting wastewater in the past decades caused severe arsenic pollution in Dieshui River basin, leading to serious problems in the human health and ecosystem.

In the nature, arsenic mainly exists in water as inorganic species (As(III) and As(V)) (Liu et al., 2014). Compared to As(V), As(III) causes much more public concerns due to its higher toxicity and lower security threshold. It is also hard to adsorb and remove As(III) for its existence as nonionic H_3AsO_3 in wastewater at pH up to 8. Although As(V) is thermodynamically stable in the presence of oxygen, As(III) is hard to be oxidized directly by oxygen. Thus, it is absolutely essential to pre-oxidize As(III) to As(V) prior to adsorption or co-precipitation of the resulting As(V). Meanwhile, adsorption removal has been considered as a feasible method to remove arsenic from solutions owing to its simplicity, sludge free operation and potential for regeneration (Jang et al., 2006; Zhang et al., 2007; Tang et al., 2008, 2014).

In recent years, nanoscale zero valent iron (nZVI) has attracted considerable attention for ex/in situ treatment of contaminants (Zhou et al., 2014; Tang et al., 2015). Compared with other adsorbents (Cheng et al., 2016; Yan et al., 2015), nZVI can adsorb As(III), transform partial highly soluble As(III) to insoluble As(V) via coupled oxidation of nZVI and Fe(II), and subsequently form the As(III)-Fe(III) and As(V)-Fe(III) precipitates (Ramos et al., 2009), but its corrosion and passivation in aquatic media greatly reduce its ability to remove arsenic (Velimirovic et al., 2014). Lv et al. prepared a series of nZVI-Fe_3O_4 nanocomposites, and found that an appropriate thickness of the Fe_3O_4 shell can improve iron corrosion and electron transfer from the Fe^0 core (Lv et al., 2011). In our previous study, it was reported that FeS@Fe^0 nanocomposites can synergistically enhance the Fe^0 corrosion with more electron transfer from Fe^0 core to the FeS surface (Tang et al., 2016).

Core-shell Fe@Fe_2O_3 nanobunches (NBZI), is synthesized by the reduction of ferric ions with sodium borohydride (Meng et al., 2011). In comparison with nZVI, NBZI is more suitable for practical application owing to the extremely high specific surface area and the existence of Fe_2O_3 shell, which can protect the material from spontaneous combustion in air, beneficial to shipping and storage. Yi et al. applied NBZI in removal of Cr(VI) (Yi et al., 2015) and found that NBZI could efficiently remove aqueous Cr(VI) by adsorption and partial reduction. Shi et al. demonstrated that NBZI can improve Fenton oxidation efficiency because it could induce single-electron molecular oxygen activation to generate $\bullet O_2^-$ and two-electron molecular oxygen activation to produce H_2O_2 by outward electron transfer from iron core to the ferrous ions and the iron oxide shell surface, respectively (Shi et al., 2014). Guo et al. found that some oxidants would promote the corrosion of zero value iron (Guo et al., 2015). Obviously, the generation of $\bullet O_2^-$ and H_2O_2 might not only increase the content of reactive oxygen species (ROSs), but also accelerate the removal of arsenic because of partial As(III) being rapidly oxidized to As(V). There is no doubt that it will be a very promising way for treatment of arsenic through oxidation, adsorption and co-precipitation by NBZI.

In this study, NBZI was applied in treatment of arsenic in acid wastewater and contaminated river sediment from Dieshui River basin caused by metallurgical industry. The mechanism of removal pathways of As(III) were proposed by using scanning electron microscopy (SEM), transmission electron microscopy (TEM), X-ray diffraction (XRD) and X-ray photoelectron spectra (XPS) to characterize the materials. The material stability experiment and the sequential extraction experiments of arsenic in the sediment were also carried out in detail. The influences of specific environmental conditions, such as pH, temperature, coexisting ion, and etc., are also considered, respectively. Furthermore, a new Fenton-Like system of NBZI/H_2O_2 to remove arsenic under the anoxic condition was also proposed.

2. Experimental section

2.1. Chemicals

The following chemicals were of analytical reagent grade, including $FeCl_3 \cdot 6H_2O$ (99%), $FeSO_4 \cdot 7H_2O$ (99%), KBH_4 (95%), $NaBH_4$ (>96%), H_2O_2 (30%w/w), HCl, NaOH, NaCl, $CaCl_2$, $NaHCO_3$, Na_2SO_4, $MgCl_2 \cdot 6H_2O$, Na_2HPO_4, *tert*-butyl alcohol (TBA). The As(III) stock solution was prepared by $NaAsO_2$ (Mallinckrodt), and all chemical solutions were made from deionized (DI) water.

2.2. River sediment and acid wastewater characteristics

Sediments were sampled from the Dieshui River, located in Shimen County, Hunan Province in the southern China. For this study, contaminated sediments (0–20 cm depth) were collected from Dieshui River (111°2′41.72″E, 29°39′36.04″N). Samples were air dried, crushed, sieved (75 μm) and stored at 4 °C prior to the experiments. Acidic wastewater containing high concentration of arsenic was taken from the sewage from a metallurgical plant situated in the same river basin.

After nitric acid digestion employing US EPA standard method (EPA3050B, 1996), the contents of metal elements in the river sediment and acid wastewater were determined by inductive coupled plasma emission spectrometer (ICP, Baird PS-6, USA), given in Tables S1–S2 in the Supporting Information.

2.3. NBZI preparation

NBZI were synthesized by the reduction of $FeCl_3 \cdot 6H_2O$ aqueous solution with $NaBH_4$ aqueous solution as previously reported with slight alteration (Lu et al., 2007; Ai et al., 2007). Briefly, 0.4 M of $NaBH_4$ was dropwise added into 0.01 M of $FeCl_3 \cdot 6H_2O$ solution, and the synthetic process was agitated by a revolving propeller. After the addition, the black fine particles were aged in water for 0, 2, 4, and 6 h, labeled as NBZI-0, NBZI-2, NBZI-4, and NBZI-6, respectively. The whole process of synthesis is simple without any protection gases or vacuum atmosphere. Finally, the synthesized materials were washed with deionized water or ethanol and then dried under nitrogen flow for characterization (Ai et al., 2013). For comparison, Fe_2O_3 nanoplates were prepared and described in T1 of Supporting information (SI). The Nanofer 25 nZVI particles (produced from nanosized ferrihydrite) in aqueous dispersion form were purchased from the NANOIRON® Company (Czech Republic, EU). The characterization methods were described in SI.

2.4. Experimental procedure

The preliminary experiments were conducted by adding 200 mg of NBZIs into 100 ml solution of 2.3 mg L^{-1} As(III) without pH adjusting. Then, the batch experiments were carried out in the anoxic and aerobic conditions by adding 5 mg NBZIs with different water aging time into 100 mL As(III) solution. The initial pH of As(III) solutions were adjusted with NaOH or HCl of 1 mol L^{-1} to 7.0 ± 0.2. Nitrogen was pumped into the solution at a rate of 1.5 L min^{-1} to remove molecular oxygen to imitate anoxic conditions in the underground environment. Aliquots of the aqueous solutions were withdrawn at intervals and then immediately passed through a 0.45 μm polytetrafluoroethylene filter for further analysis.

In order to be consistent with the simulated wastewater experiment, the raw wastewater was diluted 10 times before use and adjusted to neutral by 0.1 M NaOH. 5 mg of NBZI was added into 100 ml wastewater, and magnetically separated from the treatment solution for direct reuse in the next batch of wastewater.

As for river sediment treatment, certain amount of deionized water was added in 500 ml flask with 100 g of sediment to reach 5 cm high above the sediment surface, and stirred for 30 min. And then about 8 g NBZI was added into the mixed liquor followed by 30 min mechanical mixing. The mixtures were sealed for aging without any pH adjustment. 1 ml supernatant and 1 g sediment sample were taken from the mixed liquor for the analysis of metal fraction, respectively, at different time intervals during 20 days. All the work was done at room temperature (25 °C) unless otherwise mentioned.

2.5. Sequential extraction of sediment-sorbed arsenic

Four fractions of As in sediment were determined by the three-step selective sequential extraction (SSE) proposed by European Commission (Salomons, 2006) as follows: I) soluble species, cation exchange sites and carbonates (here defined as acid-soluble), extracted by 0.11 M acetic acid at pH 2; II) ion and manganese oxide fraction (here defined as reducible fraction), extracted by 0.5 M hydroxyl ammonium chloride at pH 2; III) organic and sulfide fraction (here defined as oxidizable fraction), extracted with hydrogen peroxide 30% and treated with 1 M ammonium acetate at pH 2; and IV) the residual fraction, the maintains in the solid (here defined as the metals in the crystalline lattice of primary and secondary minerals), extracted by aqua regia. 0.5 g treated sediment was added to a 50 ml Teflon centrifuge tube to mix with the extractants step by step. For every step, the extract fluid was poured out, filtered through a 0.45 μm filter membrane for the analysis.

3. Results and discussion

3.1. The characterization of NBZIs aging to different extents and their performance in aerobic removal of As(III)

The SEM images show the morphology of NBZI with different aging time in Fig. 1a–d. The NBZI in all the four samples look like necklace nanobunches formed by strings of irregular beads within the range of 80–500 nm. The reason for the large size of the beads compared to the reference work is that we decreased the addition rates of $NaBH_4$ to 1 mL min^{-1} (Lu et al., 2007). The TEM image of NBZI-2 reveals that the nanobunches are a kind of core-shell structure (Fig. 1e). The crystalline structures of the prepared four samples were analyzed using XRD (Fig. 1f). A clear diffraction peak at 2θ value of 44.9°, consistent with the standard pattern of metallic Fe (JCPDS, file No. 3-1050), was observed in the four NBZI samples. Meanwhile, Fe_2O_3 (Hematite, JCPDS file No. 2-915) was also found in NBZI-2 and NBZI-4. Perhaps because the content of Fe_2O_3 in NBZI-0 was too low to be detected and NBZI-6 was prepared with too long aging time, Fe_2O_3 was likely to fall off the material. In addition, the Fe^0 peak intensity of NBZI-2 and NBZI-4 gradually weakened with the increase of aging time because Fe^0 would be gradually oxidized. According to these results, we can assume that the nanobunches were of Fe^0 core surrounded by a layer of iron oxide shell.

The reactivity of these four NBZI samples was assessed by the aerobic removal of As(III). As shown in Fig. 2, about 89% of As(III) was removed by NBZI-0, NBZI-4 and NBZI-6 in 120 min, while NBZI-2 showed higher efficiency of 96.5% (Fig. 2a). The removal data fit well with the pseudo-second order kinetic model (Fig. 2b). The removal rate constants (k_{As}) of NBZI-0, NBZI-4 and NBZI-6 show no significant difference (Table 1). However, the removal rate of NBZI-2 is nearly 25 times as much as that of NBZI-4. These results indicate that water aging process was able to greatly affect the performance of NBZI in aerobic removal of As(III).

In general, nZVI spontaneously reacts with oxygen to produce Fe^{2+} and Fe^{3+} in aqueous phase, along with hydroxides, iron oxides and oxyhydroxides formed under aerobic condition (Kanel et al., 2005; Manning et al., 2002). Moreover, As(III) may be captured by the matrix of the growing corrosion product and then be removed from the solution via precipitation and co-precipitation (Kanel et al., 2006; Noubactep, 2008). Additionally, Fe_2O_3 is also a highly efficient adsorbent, and its adsorption of As(III) is mainly dominated by the electrostatic attraction force in the early stage and then the covalent bonding force in the late stage (Du et al., 2013). It was initially expected that with aging time prolonging, the amount of centric nZVI decreased, accompanying with the increasing thickness of iron oxide shell and ferrous ions leaching, which would be beneficial to the removal of As(III) if these three sections were maintained in a proper proportion. On the other hand, the rate of nZVI corrosion would become slower with the iron oxide shell thickness increasing because the excessively thick shell could block the electron transfer. It would decrease the removal efficiency of As(III). In our study, NBZI-2 performed the highest absorption ability among these NBZI particles, so it was used in further experiments. The adsorption capacity of NBZI-2 reached to 189 mg g^{-1} under aerobic at neutral pH, 60 times as that of nZVI under the identical conditions (Table 2).

3.2. Analysis of the role of NBZI core-shell structure in As(III) removal

In order to reveal the super high adsorption capacity under aerobic and anoxic conditions, the contribution of each component (Fe^{2+}, Fe_2O_3 and nZVI) of the special structure of NBZI (Fig. 3) in the removal process was carefully investigated and compared. We found that neither Fe^{2+} nor Fe_2O_3 alone could effectively remove As(III), and there is no obvious improvement in As(III) removal using both of these two materials, whether in the anoxic or aerobic environment. However, any of them in combination with nZVI could greatly improve the removal ability. Especially when the three components were combined together, the removal efficiency reached to 88% and 49% under the aerobic and anoxic condition, respectively (Fig. 3a and b). Nevertheless, the removal capacity is still less than that of NBZI-2, although the dosing amount of the mixture is already 3 times of NBZI-2, which reveals that there might be a synergetic effect among Fe^0 core, Fe_2O_3 shell and Fe^{2+} on the removal of As(III) by NBZI-2. In order to prove the supposition, we compared the concentration changes of Fe^{2+} and Fe^{3+} released from NBZI-2 and nZVI under the aerobic conditions, and found that the special structure of NBZI-2 accelerate the corrosion of nZVI (Fig. S1 in the SI). The concentrations of Fe^{2+} and Fe^{3+} increased significantly in the first 30 min, and then the concentrations apparently declined because of the precipitation and oxide formation of ferric ions at pH > 4.0, which is beneficial to the removal of As(III).

During the As(III) removal process in the presence of oxygen, adsorption and oxidation should be both taken into account, because Fe^0 could react with molecular oxygen to produce reactive oxygen species (Keenan and Sedlak, 2008; Que and Tolman, 2008). Ai et al. found that Fe@Fe_2O_3 nanobunches showed interesting core-shell structure dependent reactivity on the aerobic removal of 4-chlorophenol, which proves the two-electron molecular oxygen activation pathway via the outward electron diverted from Fe^0 core to the iron oxide shell surface, and single-electron molecular oxygen activation via ferrous ions bound on the iron oxide shell (Ai et al., 2013). The oxidation of Fe^0 to ferrous ions is considered to be accompanied with the two-electron transfer to O_2 to generate H_2O_2 (Eq (1)), which could react with ferrous ions to produce •OH with strong oxidation capability under acidic to neutral pH conditions (Eq (2)). This two-electron molecular oxygen activation

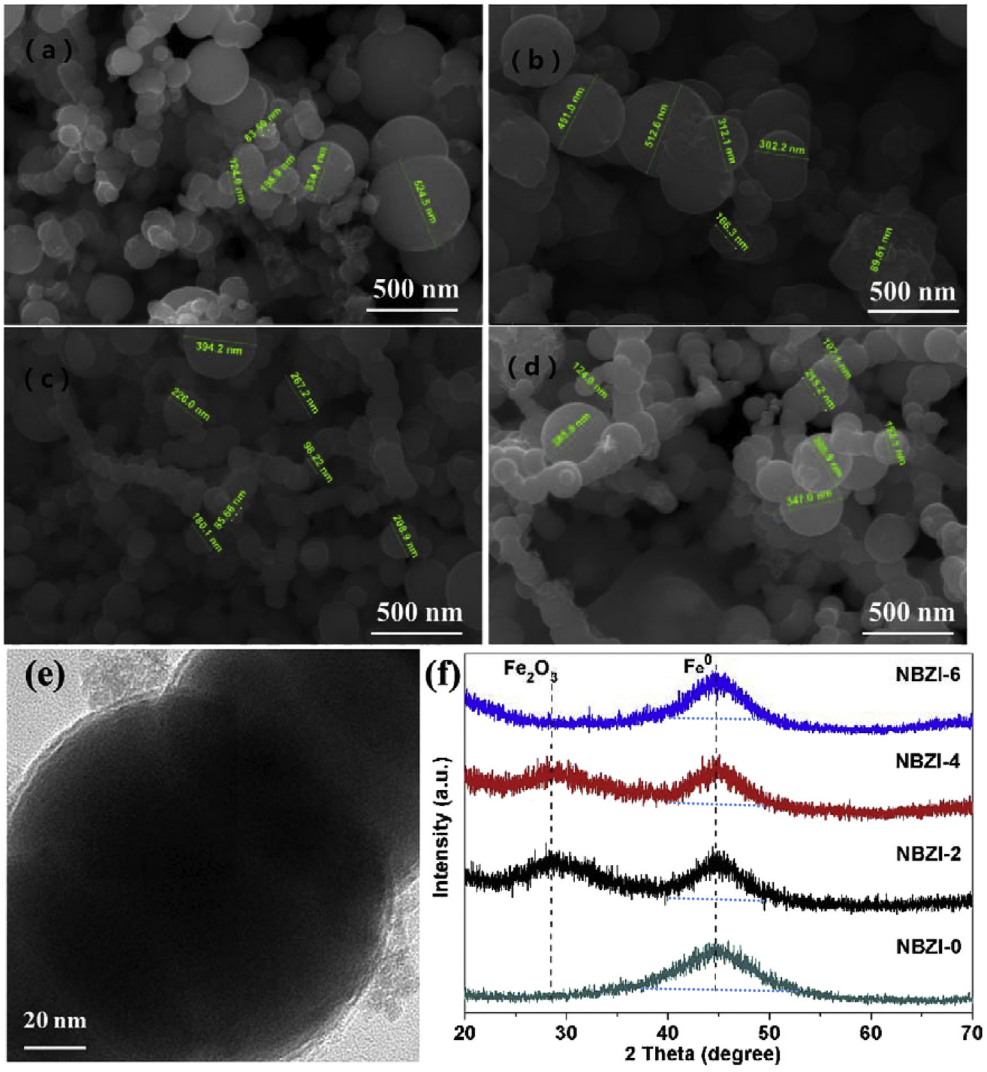

Fig. 1. SEM images of NBZI-0(a), NBZI-2(b), NBZI-4(c) and NBZI-6(d); TEM images of NBZI-2 (e); and XRD patterns of the NBZI (f).

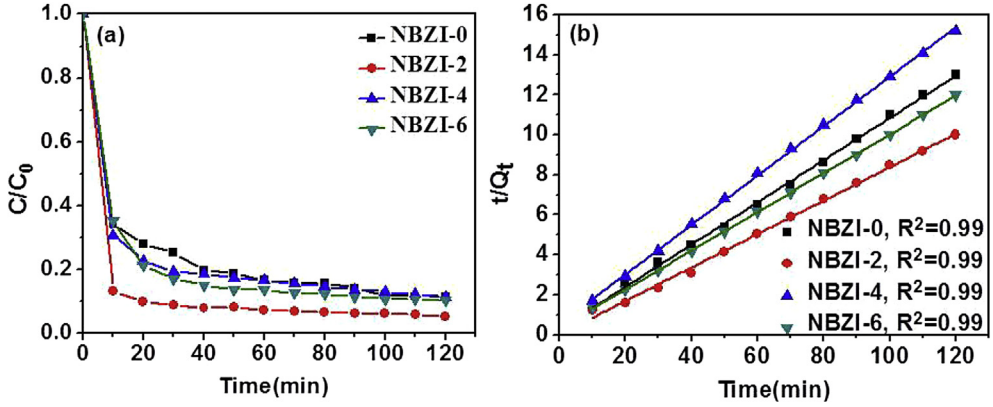

Fig. 2. (a) Efficiency of As(III) removal by materials with different aging time in the presence of oxygen; (b) plots of t/Q_e versus time for the aerobic removal of As(III). Initial NBZI = 200 mg L^{-1}, initial As(III) = 2.3 mg L^{-1}.

Table 1
The difference between the removal rates constants (k_{As}) over NBZI.

Sample	NBZI-0	NBZI-2	NBZI-4	NBZI-6
k_{As} g/(mg min)	0.0373	0.7270	0.0289	0.0281

process starts from electron transfer from iron core of NBZI to the surface of iron oxide shell, where the adsorbed electrophilic molecular oxygen could capture the electrons. Obviously, the iron oxide shell could influence the electron transfer process and also

Table 2
Maximum arsenic adsorption capacity (mg/g) of some adsorbents reported in the literature compared with NBZI-2.

Material	pH	As(III) removal mg/g	reference
NBZI-2	7	189	This work
Bare nZVI	7	3.50	(Kanel et al., 2005)
ZVI/Starbon	7	26.8	(Baikousi et al., 2015)
Activated Carbon/nZVI	6.5	18.2	(Zhu et al., 2009)
Iron containing ordered mesoporous carbon	6.5	9.3	(Gu et al., 2007)
nZVI-RGO nanoparticles	7	35.8	(Wang et al., 2014)
Iron oxyhydroxide-loaded cellulose beads	7	99.6	(Guo et al., 2015)
α-Fe_2O_3 nanowires deposited diatomite	3.5	60.6	(Du et al., 2013)
ultrafine magnesium ferrite nanocrystallites	7	127.4	(Tang et al., 2013)

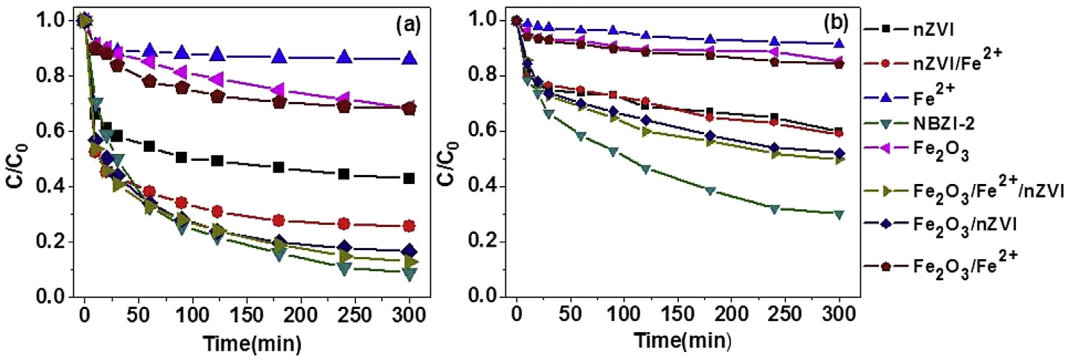

Fig. 3. Removal of As(III) in different reaction systems under aerobic (a) and anoxic (b) conditions. The concentration of Fe^{2+}, H_2O_2, Fe_2O_3 and As(III) were 50 mg L^{-1}, 8×10^{-5} mol L^{-1}, 50 mg L^{-1} and 2.3 mg L^{-1}, respectively; the concentration of NBZI was 50 mg L^{-1}; the volume of the pollutant solution is 100 ml; the initial pH was 7.0.

verify what we previously discussed that water aging process would affect aerobic removal of As(III), because iron oxide shell is becoming thicker with prolonged water aging, which would impede the electron transfer. Simultaneously, the ferrous ions ($\equiv Fe^{III}OFe^{II}OH/\equiv Fe^{II}OFe^{III}OH$) bound on the surface of iron oxide could activate oxygen molecule via single-electron reduction pathway to produce reactive oxygen species (Eqs (3)–(5)). The study also further explains the reason why the core-shell structure promoted the corrosion of nZVI compared to the bare nZVI. Meanwhile, As(III) oxidation can occur after it is adsorbed onto the surface of iron (hydr)oxide, and aqueous As(III) can also be oxidized by reactive oxygen species such as •OH and $•HO_2$ in the presence of oxygen, accompanied by a subsequent adsorption of As(V) on iron (hydr) oxide (Han et al., 2016).

$$Fe^0 + O_2 + 2H^+ \rightarrow Fe^{2+} + H_2O_2 \quad (1)$$

$$Fe^{2+} + H_2O_2 \rightarrow Fe^{3+} + •OH + OH^- \quad (2)$$

$$\equiv Fe^{III}OH + Fe(II) + H_2O \rightarrow Fe^{III}OFe^{II}OH + 2H^+ \quad (3)$$

$$\equiv Fe^{III}OFe^{II}OH \rightarrow Fe^{II}OFe^{III}OH \quad (4)$$

$$\equiv Fe^{III}OFe^{II}OH/Fe^{II}OFe^{III}OH + O_2 \rightarrow Fe(III) + •O_2^- \quad (5)$$

3.3. Comparison of the anoxic and oxic As(III) removal

The effect of oxygen molecules on As(III) removal by NBZI-2 was studied by comparing the aerobic and anoxic As(III) adsorption capacity in solution at initial pH of 7.0 ± 0.2 (Fig. 4). In aerobic conditions, the removal efficiency of As(III) with lower concentrations reached up to 92% in 300 min (Fig. 4a). When the concentration of As(III) increased from 2.3 mg L^{-1} to 12.5 mg L^{-1}, the removal efficiency of As(III) dramatically decreased from 92% to 75.5% under aerobic conditions, and the adsorption equilibrium time extended to 1200 min (Fig. 4b). Although the adsorption rate decreased, the total adsorption amount increased, indicating an adsorptive saturation at a high aqueous As(III) concentration. The increasing concentration of As(III) would provide impetus to move As(III) from the aqueous solutions using NBZI-2 due to more valid collisions between As(III) and the active sites on NBZI-2. Similar phenomena were also obtained in other studies (Weng et al., 2006; Giasuddin et al., 2007).

However, a control experiment showed that NBZI-2 could not exhibit high As(III) removal efficiency in the absence of oxygen. As we can see in Fig. 4a and b, the removal efficiency of As(III) remarkably reduced to 68.0% and 63.5% under the anoxic conditions with low and high As(III) concentrations, respectively. Apparently, the presence of oxygen could improve As(III) removal capacity of NBZI-2 at neutral pH. The impact of solution pH on the adsorption of As(III) under anoxic and aerobic is discussed detailedly in T5 in SI. Generally speaking, nZVI would react with H_2O and O_2 to generate iron oxides and hydroxides in the presence of oxygen, as Eqs (6)–(9). The ferric hydroxide in aqueous solutions can also adsorb arsenic by co-precipitation as well as complexation. The corrosion of nZVI would release ions under the anoxic condition. Without the effect of oxygen, iron mainly exists in the form of dissolved ferrous ions in the aqueous solutions, as in Eq (10). The whole process could only produce little or only a small amount of ferric hydroxide, which indicated that removal of As(III) can be considered as inner-sphere complexation with the iron oxides. Compared with the reaction mentioned above, we also found the ratio of surface absorbed oxygen species to iron oxides (the O_{OH}/OFe_2O_3) declined from 3.56 to 1.82 (Fig. 5a) under the aerobic condition, indicating that more Fe-As oxides existed on the reacted $Fe@Fe_2O_3$ nanobunches. Meanwhile, Keenan et al. reported that

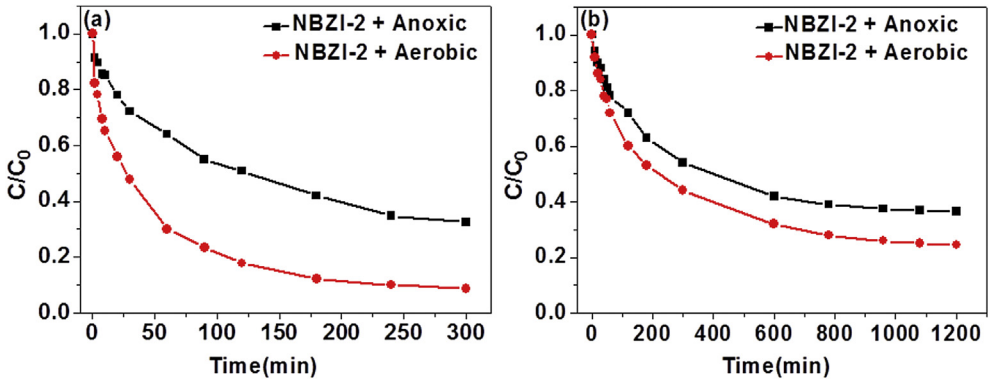

Fig. 4. Comparison of the As(III) removal by NBZI with low and high concentrations of As(III) under anoxic and aerobic conditions. (a) Low concentration of As(III) (initial As(III) = 2.3 mg L^{-1}). (b) High concentration of As(III) (initial As(III) = 12.5 mg L^{-1}; initial NBZI = 50 mg L^{-1}).

removal of arsenic on the corroded iron surface was the primary mechanism by nZVI in the presence of oxygen (Keenan and Sedlak, 2008). Kanel et al. also proposed that over four-fifths of non-stabilized ZVI particles were iron oxides, and they confirmed that the shell iron oxides adsorbed arsenic through inner-sphere complexation (Kanel et al., 2006). It also means that forming complex compound with iron oxides plays a leading role in the removal of As(III), which is consistent with the results under the anoxic condition.

$$Fe^0 + O_2 + 2H_2O \rightarrow Fe^{2+} + H_2 + 2OH^- \quad (6)$$

$$4Fe^{2+} + 2H_2O + O_2 \rightarrow 4Fe^{3+} + 4OH^- \quad (7)$$

$$6Fe^{2+} + O_2 + 6H_2O \rightarrow 2Fe_3O_4(s) + 12H^+ \quad (8)$$

$$Fe_3O_4(s) + O_2 + 18H_2O \leftrightarrow 12\ Fe(OH)_3(s) \quad (9)$$

$$2Fe^0 + 2H_2O \rightarrow 2Fe^{2+} + H_2 + 2OH^- \quad (10)$$

As mentioned above, NBZI-2 shows inferior removal ability of As(III) under anoxic conditions than in aerobic conditions. In order to further enhance the performance of NBZI-2 in the absence of oxygen, we introduced H_2O_2 to combine with NBZI-2 in the treatment process referring to traditional Fenton reaction. In contrast with the low efficiency in As(III) removal by traditional Fenton reaction, the coupling of H_2O_2 with NBZI-2 resulted in a very rapid and highly efficient removal of As(III) (Fig. 6a and b). We found that H_2O_2 alone are not able to oxidize As(III), and addition of ferrous ions could improve the removal rate to reach nearly 50% and 53% under anoxic and aerobic conditions, respectively. However, the practical application of Fenton reaction is still restricted by its narrow working pH range (2.5–4) (Yi et al., 2015), because the low oxidation ability and easy formation of insoluble ferric products at pH > 4.0. Compared to the bare NBZI-2, the removal capacity of As(III) by combining NBZI-2 with H_2O_2 increased to 100% and 90% under aerobic and anoxic conditions, respectively. Guo et al. found that some oxidants can react with nZVI surface at high rate with high stability, driving intensive and rapid iron corrosion accompanied by the generation of continuous production of iron oxide and oxyhydroxides (Guo et al., 2015). The oxidants have been extensively used in industrial waste water and contaminated groundwater treatment with significantly higher solubility than O_2, which greatly improves their diffusion through the liquid/solid interface and the subsequent surface reaction. The H_2O_2 added into NBZI-2 system can be completely consumed within 30 min in the removal of arsenic, indicating that they can rapidly oxidize iron and facilitate the corrosion of nZVI (Guo et al., 2015). The violent surface reaction between oxidants and NBZI-2 generated a great deal of iron oxyhydroxides, such as hematite, goethite, magnetite and various amorphous phases of iron oxides/hydroxides. These iron oxides play a critical role in As(III) removal through multiple mechanisms including adsorption, precipitation, and co-precipitation (Appelo et al., 2002; Konthur et al., 2013). The new system provides a new approach for the efficient and rapid removal of As(III) in the surface water and the ground water.

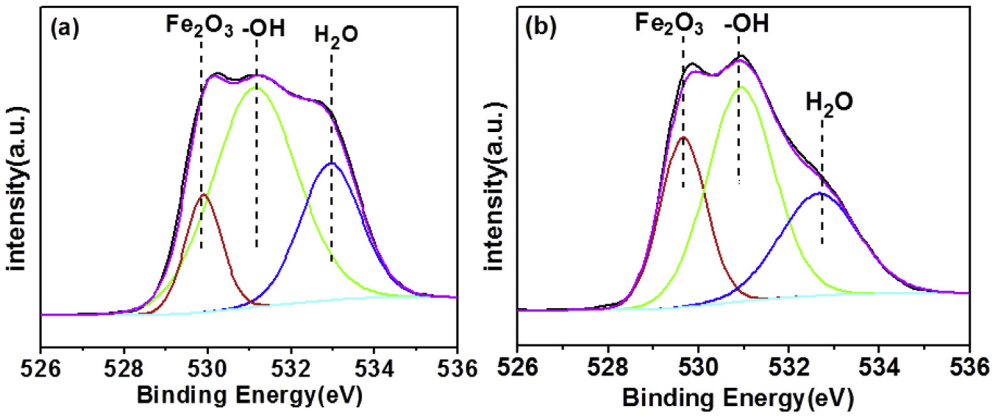

Fig. 5. XPS responses of (a) O1s before reaction with As(III) and (b) O1s after reaction with As(III).

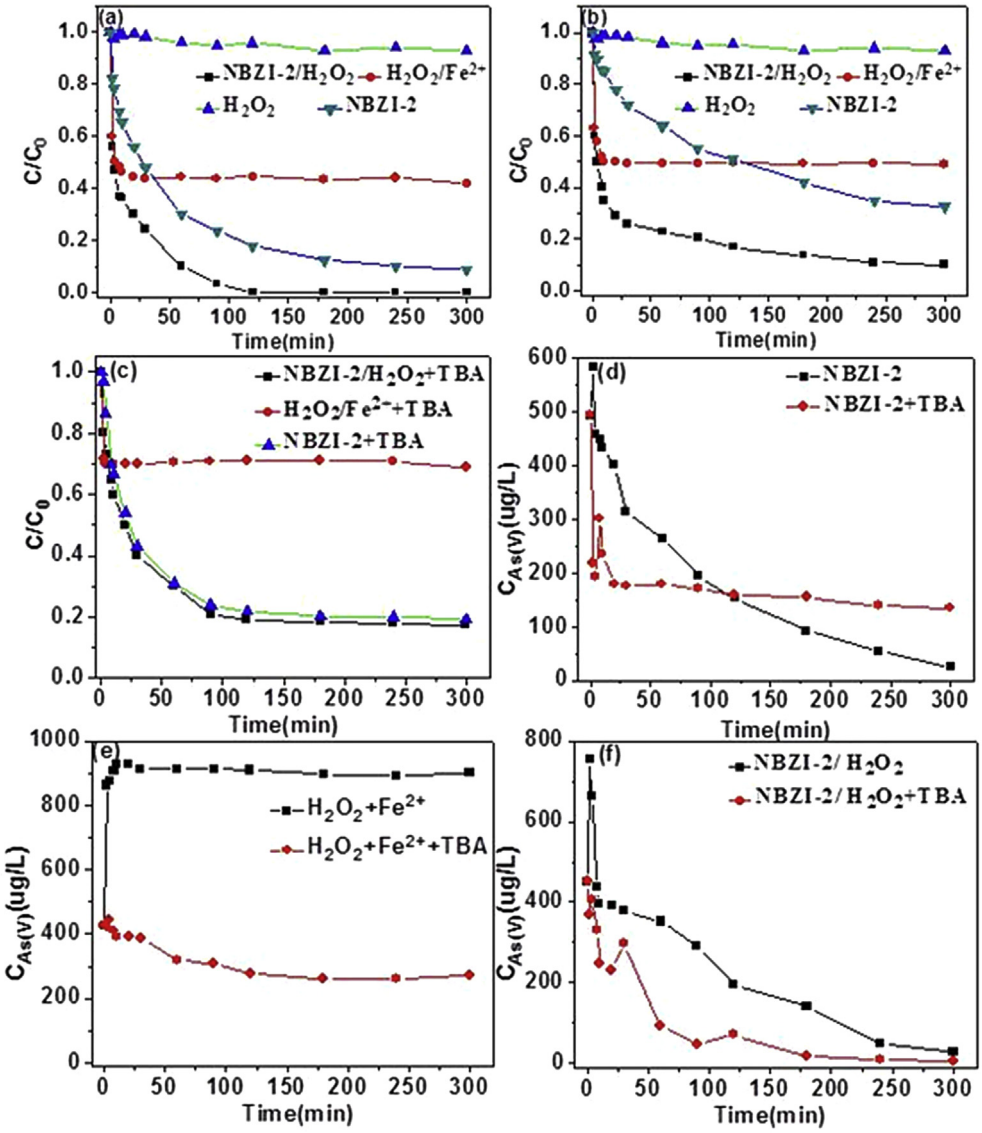

Fig. 6. The anoxic (a) and aerobic (b) removal of As(III) by different systems; Aerobic removal of As(III) in the presence of TBA by different systems (c); Changes of the concentrations of As(V) generated during As(III) oxidation by NBZI system (d), H_2O_2/Fe^{2+} system(e), and NBZI/H_2O_2 system (f) in the presence of air; initial NBZI = 50 mg L^{-1}, initial As(III) = 2.3 mg L^{-1}.

As(III) might be oxidized by hydroxyl radicals during the Fenton reactions. We therefore employed active species trapping experiments to check if hydroxyl radicals were generated in NBZI-2/H_2O_2, H_2O_2/Fe^{2+}, and bare NBZI-2 system by using tert butyl alcohol (TBA) as •OH scavenger under the aerobic conditions (Fig. 6c). The comparison of the inhibitory effects on the three systems for the pollutant removal could reflect whether hydroxyl radicals were generated. Obviously, the pollutant removal efficiencies of NBZI-2/H_2O_2 and H_2O_2/Fe^{2+}systems were decreased by 20%, and that of bare NBZI-2 system only declined by 10%. Meanwhile, we also studied the changes of aqueous As(V) with or without adding TBA (Fig. 6d, e and f), and discovered that all of the three systems would rapidly oxidize As(III) to As(V) in the aqueous solution. However, the oxidation ability of NBZI-2/H_2O_2 system was significantly higher than that of H_2O_2/Fe^{2+} and bare NBZI-2 system. As we discussed in the previous section, NBZI-2 was easier for oxidation corrosion and released larger amount of ferrous ions than nZVI, and then adding of H_2O_2 would generate more hydroxyl radicals. Based on these results, we conclude that the hydroxyl radicals play a vital role in the As(III) removal, and the new system not only promotes the corrosion of Fe^0, but also improves the oxidation ability.

3.4. Adsorption kinetics and adsorption isotherm

The kinetics of As(III) removal were investigated with low or high initial As(III) concentration in the presence of 50 mg L^{-1} NBZI-2 at pH 7.0 ± 0.2. Under the aerobic conditions, the adsorption capacity of NBZI-2 increased from 42.3 to 189.0 mg g^{-1} with initial As(III) concentration increased from 2.3 to 12.5 mg L^{-1} (Fig. S5), indicating an adsorptive saturation at a high aqueous As(III) concentration. With the increasing concentration of As(III), this would provide higher impetus for As(III) to move from the aqueous solution to NBZI-2, leading to more collisions between As(III) and active sites on NBZI-2. In the absence of oxygen, the adsorption amount of NBZI-2 showed lower value, 35.0 mg g^{-1} and 149 mg g^{-1} with low and high As(III) concentrations, respectively. However, the pseudo-second order adsorption kinetics model fits these experimental data obtained in both anoxic

and aerobic conditions, with high correlation coefficients ($R^2 \approx 0.99$) and good linearity, indicating that chemisorption governs the adsorption process. The result corresponds to many previous reports for As(III) removal using similar iron materials (Zhu et al., 2009; Gu et al., 2007). The specific fitting results of the adsorption kinetics are presented in Table 3. The removal rate increased with higher initial concentration of As(III). At the same As(III) concentration, the adsorption rate at least increased by 2 orders of magnitude when the initial NBZI-2 concentration increased from 50 mgL^{-1} to 200 mg L^{-1}. Obviously, the result indicates that the adsorbent amount and initial As(III) concentration deeply influence the adsorption rate.

Adsorption isotherm plays a critical role in optimizing the use of adsorbent, since it can reveal the adsorption capacity of adsorbent and describe how the adsorbent interacts with adsorbate. Two typical isotherm models, Langmuir and Freundlich isotherms, are tested to explain the As(III) adsorption behavior (Fig. S6). The As(III) removal process fits better with the Langmuir model with correlation coefficient R^2 values of 0.99, indicating that the As(III) adsorption is a monolayer coverage (Table 4). The calculated Q_{max} value, which represents the adsorption ability of the adsorbent, is 195 mg g^{-1}. Compared with other materials, we have never known any iron-based material holding such high adsorption capacity like NBZI-2 in As(III) removal. Also, some literature data are summarized in Table 2, concerning the As(III) adsorptive capacities of other adsorption materials. Meanwhile, we also found that the removal efficiency decreased when the temperature increased from 298 K to 308 K. It can be explained by that the mobility of ions will increase along with the rise of the reaction temperature (Wang et al., 2014), and the electrostatic interactions and surface complexation may decline when the temperature increased.

Table 4
Calculated equilibrium constants for As(III) adsorption onto NBZI-2.

Isotherms	Temperatures (K)	Parameters			
		q_{max}	k_L	R^2	R_L
Langmuir	298	195.81	0.775	0.9905	0.091
	308	175.27	0.546	0.9924	0.295
		n	k_f	R^2	
Freundlich	298	0.187	111.19	0.9257	
	308	0.234	84.69	0.8984	

3.5. Removal of arsenic in acid wastewater and polluted sediment

The removal of arsenic from acid wastewater was also tested in the aerobic and anoxic condition, respectively. The total arsenic removal efficiency reached 100%, 80%, 50%, and 100%, 60%, 50% by 50, 100, and 200 mg L^{-1} NBZI-2, in the aerobic and anoxic conditions, respectively (Fig. 7a and b). It shows that complete removal of As(III) from the real water samples needed a higher dosing amount of NBZI-2 compared to the simulated wastewater, possibly due to the presence of dissolved phosphate, organic carbon and sulfate in the actual water samples. The impacts of various cations and anions on the adsorption of arsenic are discussed detailedly in T5 in SI. Meanwhile, in order to further verify the stability of materials in practical application, we also carried out stability tests. The total arsenic removal efficiency by NBZI reached 78% after recycling 9 times; however, the removal capacity of nZVI was gradually quenched (Fig. 7c and d). This is consistent with the above discussion, and these results indicate that NBZI could be alternative to nZVI for removing arsenic in wastewater.

Speciation of arsenic in the sediment plays a vital role on its bioavailability (Fonti et al., 2015). In general, the availability and mobility of arsenic increases in the order of acid-soluble forms > reducible forms > oxidizable forms > residual forms (Soylak, 2015). The residual fractions in the sediment were of durable solid phase and difficult to be extracted and residual metal complexes have been deemed as insert and inaccessible to biota. To better understand and highlight the effect of the proposed material on the transformation of arsenic forms and to estimate the level of their stabilization, fractionation of arsenic in the sediment was performed. Changes in arsenic fraction owing to NBZI applications were confirmed after 20 days of incubation (Fig. 8), and significant changes of arsenic forms in the sediment was noted. It was found that the residual fraction concentration of arsenic increased from 80.7 ppm to 300 ppm after 20 days of incubation (Fig. 8d). Meanwhile, we also found that the arsenic released into the supernatant from polluted sediment decreased after treatment by NBZI (Fig. S7). These findings exhibited that the stabilization of NBZI was quite durable. It can greatly reduce the release of heavy metals to the environment by weakening the active arsenic fractions though it is unable to remove arsenic from sediments, the same as the accepted application of the zeolites or other materials to the remediation of heavy metal contaminated sediments (Wen et al., 2016; Zhang et al., 2007; Yang et al., 2015).

3.6. The mechanism

NBZI-2 before and after reaction was further analyzed using the X-ray photoelectron spectroscopy (XPS) technique to reveal changes of the compositions on the material surface. The XPS spectra confirmed that the prepared NBZI contains the elements Fe, C and O (Fig. 9a). The C 1s peak at 284.5 eV could be explained by the adventitious carbon on the surface of the materials. In contrast to the full survey of As(III) before reaction, we found a weak characteristic peak of arsenic at 45.5 eV after reaction, which indicates that the arsenic was adsorbed on the surface of treated NBZI-2. Various valence states of iron, Fe^{III}, Fe^{II}, and Fe^0, coexisted in NBZI (Fig. 9b). The corresponding Fe 2p peaks at binding energies of 710.8 and 724.2 eV could be ascribed to Fe^{II}, and peaks at 713.1 and 727.2 eV could be ascribed to Fe^{III}. The peaks located at 706.9 and 719.5 eV could be ascribed to Fe^0. The ratios of ferrous iron to total iron (Fe^{II}/Fe_{total}) and ferric iron to total iron (Fe^{III}/Fe_{total}) are 0.622 and 0.165, respectively. In the aging process, the iron oxide shell would be formed through the reaction of Fe^0 with water and dissolved oxygen, and then release ferrous ions to the solution. Then,

Table 3
Parameters of the pseudo first-order and second-order kinetic models for the adsorption of As(III) on the NBZI-2.

Concentrations (mg/L)	$q_{e,exp}$ (mg/g)	Pseudo-first-order modal			Pseudo-second-order model		
		$q_{e,cal}$ (mg/g)	k_1 (1/min)	R^2	$q_{e,cal}$ (mg/g)	k_2 g/(mg·min)	R^2
2.3 (N_2)	35.0	30.2	1.27×10^{-2}	0.95	34.5	1.3×10^{-3}	0.99
(O_2)	42.3	31.8	1.66×10^{-2}	0.98	43.4	1.42×10^{-3}	0.99
12.5 (N_2)	149	130.3	3.98×10^{-3}	0.97	149.2	5.8×10^{-5}	0.99
(O_2)	189	164.0	3.91×10^{-3}	0.99	190	4.5×10^{-5}	0.99

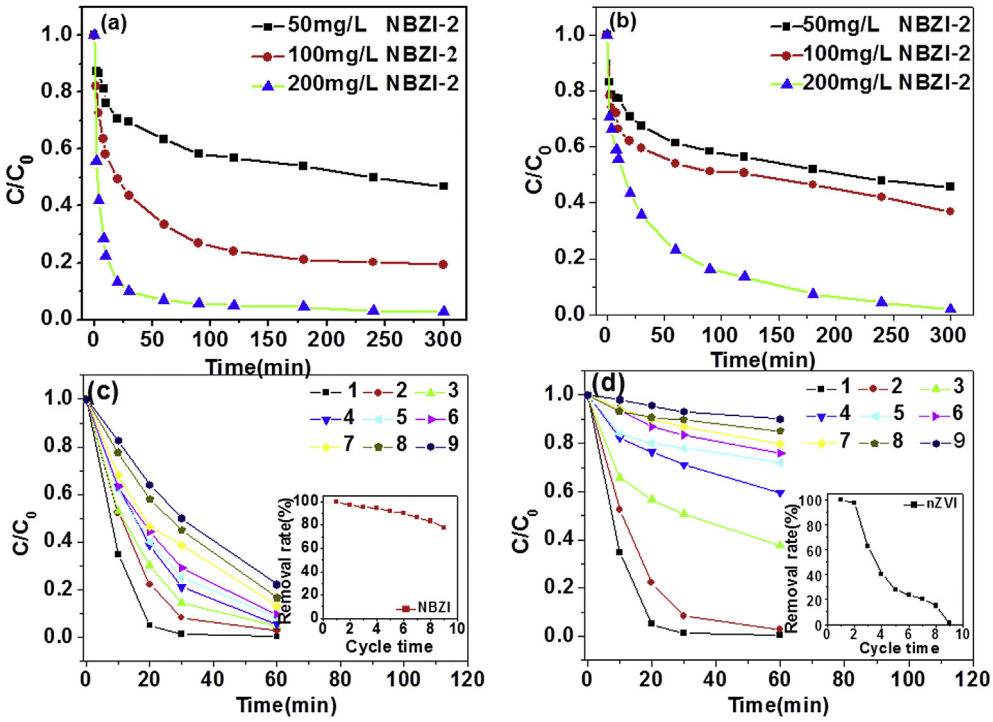

Fig. 7. Removal of total arsenic from acid wastewater using NBZI under (a) aerobic (b) anoxic conditions; (c) Removal of total arsenic using NBZI (c) and nZVI (d) for acid wastewater after different cycle times. Change of removal rate of total arsenic after different cycle times. Initial NBZI = 50 mg L^{-1}.

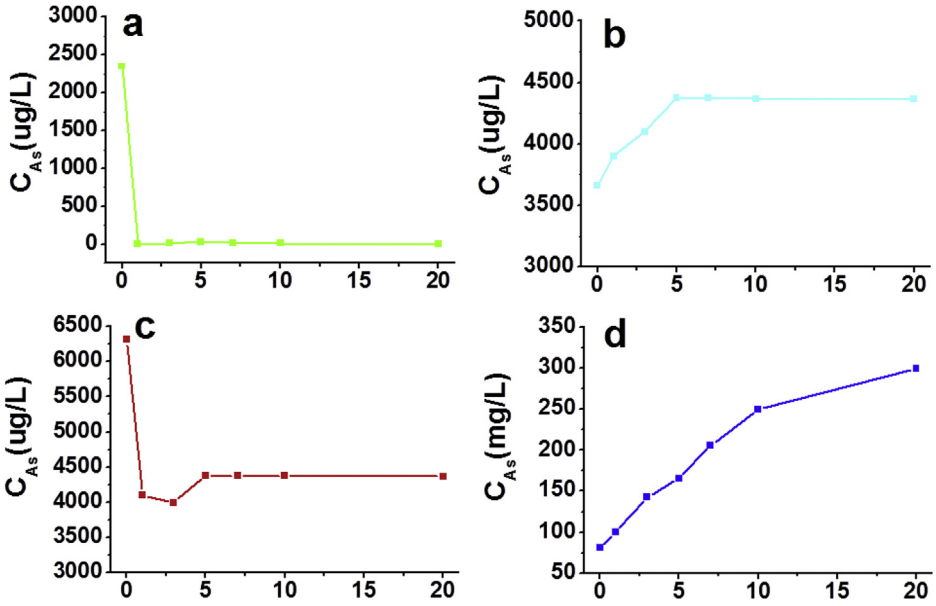

Fig. 8. The concentration of acid-soluble (a), reducible (b), oxidizable (c), and residual (d) arsenic extracted from sediment during treatment by NBZI; 5 g NBZI was added to 100 g sediment.

the oxide shell would absorb the leached ferrous ions, resulting in the increasing content of ferrous ions of NBZI. In addition, three peaks at binding energies of 529.8, 531.2 and 532.9 eV fitted the high-resolution XPS spectra of O 1s well (Fig. 5a). The peak at 529.8 eV is attributed to the lattice oxygen binding with Fe (Fe_2O_3), while the others peaks at around 531.2 and 532.9 eV suggest the presence of −OH, and H_2O on the surface (Lu et al., 2007; Zhou et al., 2014). The peak area values of −OH is higher than other species indicating existence of more metal hydroxides, such as FeOOH on the surface of NBZI. The ratio of surface absorbed oxygen species to total oxygen (O_{OH}/O_{total}) and oxygen in oxides to total oxygen (O_{Fe2O3}/O_{total}) are 0.623 and 0.175, respectively. Earlier studies have suggested that As(III) and As(V) can form inner sphere bidentate surface complexes with the surface bonded −OH(Manning et al., 2002; Farrell et al., 2001). The hydroxyl group at NBZI interface can combine with the aqueous arsenic to form surface complexes and subsequently remove arsenic from the aqueous phase. Therefore, the XPS analyses of NBZI also indicated that

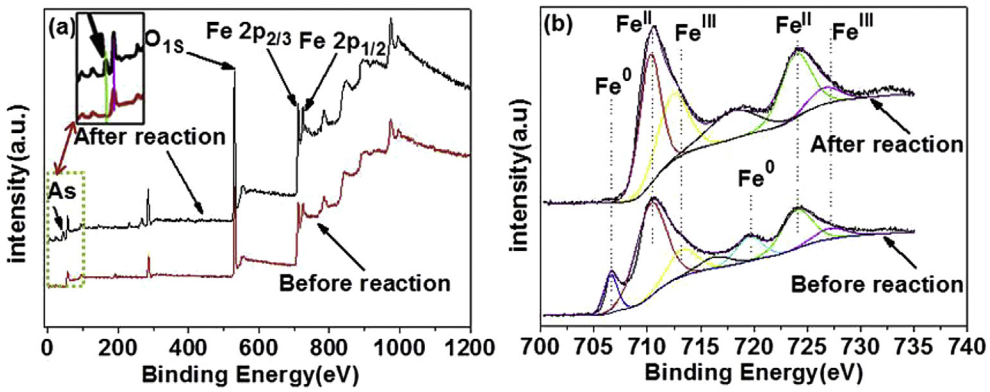

Fig. 9. XPS response of full survey (a) and (b) detailed survey of the region of Fe2p for NBZI before and after reaction with As(III) under aerobic conditions.

Fe@Fe_2O_3 nanobunches would efficiently remove aqueous arsenic. XPS was also used to identify arsenic oxidation states on iron (hydr) oxide under aerobic conditions, and the peak positions were determined by comparison to As3d binding energies reported in the literature (Ramos et al., 2009). The peaks of As(III) and As(V) were clearly surveyed on reacted NBZI-2 in the presence of oxygen. The As3d peak for each chemical state has two unresolved components owing to spin-orbit splitting corresponding to the $As3d_{5/2}$ (at lower BE) and $As3d_{3/2}$ (at higher BE) peaks separated by 0.7 eV (Fig. 10). The relative abundance of each oxidation states of arsenic can be quantified from the respective peak areas. In our study, we observed that oxidation of both As (III) and Fe (II) took place immediately after the addition of NBZI (Fig. 6a and Fig. S1). Due to the rapid oxidation of Fe (II) and formation of Fe (oxyhydr)oxides at neutral pH, more aqueous As(III) can be removed before oxidation, and then the residual As(III) will be oxidized to As(V) and adsorbed on As(V) on Fe (oxyhydr)oxides, which may be the reason why As (III) can't be completely oxidized. The same phenomenon can be seen in previous report (Han et al., 2016). Meanwhile, nearly 35% As(III) was oxidized to As(V) on the surface of iron (hydr) oxide under aerobic condition and indicated that the rapid formation of Fe (oxyhydr)oxides removes more aqueous As (III) before its further oxidation to As(V).

Based on the above analyses and results, we presented the possible mechanism for the removal of arsenic under the aerobic and anoxic conditions with NBZI-2. As we can see in Scheme 1, in the presence of oxygen, NBZI-2 can activate dissolved molecular oxygen by both single-electron transfer reaction from the surface bound ferrous ions to oxygen to produce $\cdot O_2^-$, and by two-electron transfer route from the Fe^0 core to oxygen to generate H_2O_2. The generated H_2O_2 can react with the ferrous ions to produced ·OH, and the generated $\cdot O_2^-$ can either further convert to H_2O_2 or ·OH (Yi et al., 2015), which will oxidize As(III) to As(V). On one hand, As(V) exists as oxyanions ($H_2AsO_4^-$ and $HAsO_4^{2-}$) at neutral pH (6.1–7.0), while NBZI-2 possesses positive charge, which is conducive to the promotion of arsenic removal since the increased electrostatic attraction with anionic arsenic species, hence resulting in more readily adsorption. On the other hand, compared to nZVI, the increase of electron transfer also rapidly promotes the corrosion rate of Fe^0. The corrosion product of iron oxide will react with arsenic to produce inner-sphere complexation, and the generation of iron hydroxide can also adsorb arsenic by co-precipitation (Kanel et al., 2006). Furthermore, due to this particular/unique core shell structure, the formation of oxide shell impeded superficial oxidation and passivation of NBZI during drying, storage, shipping and application process, which guaranteed the sustained activity of the system and wide application. In the absence of oxygen, when NBZI was exposed to the aqueous As(III) solution, electrostatic attraction and repulsion are not dominant, only the complexation adsorption with iron oxides played the important role due to rare oxidation of As(III) to As(V), and that As(III) only exists as H_3AsO_3. However, the removal ability of arsenic by NBZI under the anoxic condition was further improved when introducing H_2O_2. Different from other studies, NBZI in our study acts as a catalyst, H_2O_2 acting as a precursor to generate ·OH to oxidize As(III) to As(V). It was demonstrated that a significant fraction of As(III) was oxidized to As(V) in our NBZI-2/H_2O_2 system. Compared to the previous ZVI/oxidants coupling system, the new system can not only drive rapid and continuous nZVI corrosion, but also perform better oxidation ability than that of Fenton system. The expense of simple combination of NBZI-2 with H_2O_2 would have the potential to become an effective method for the purification of arsenic contaminates in groundwater.

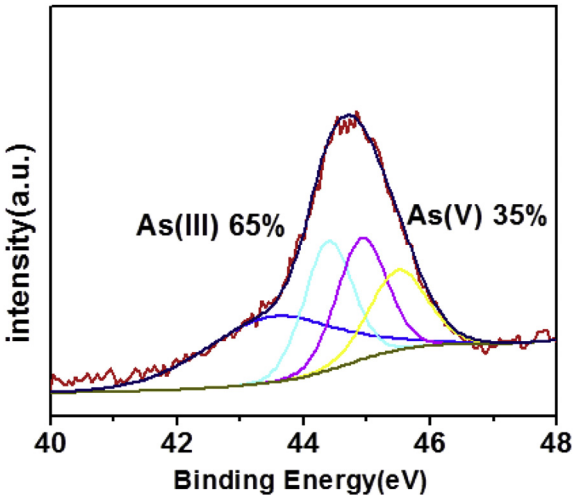

Fig. 10. As3d XPS spectra of NBZI after reaction with As(III) and As(V).

4. Conclusion

In this study, the results have shown that the addition of NBZI was effective in immobilizing arsenic in contaminated sediment, leading to an increased (or bigger) residual fraction of arsenic and a decline of the bioavailability of arsenic. Moreover, compared to nZVI, NBZI has better cycle stability and stronger capacity in the removal of arsenic in acid wastewater, which can not only decrease the toxicity by oxidation of As(III), but also effective removal the

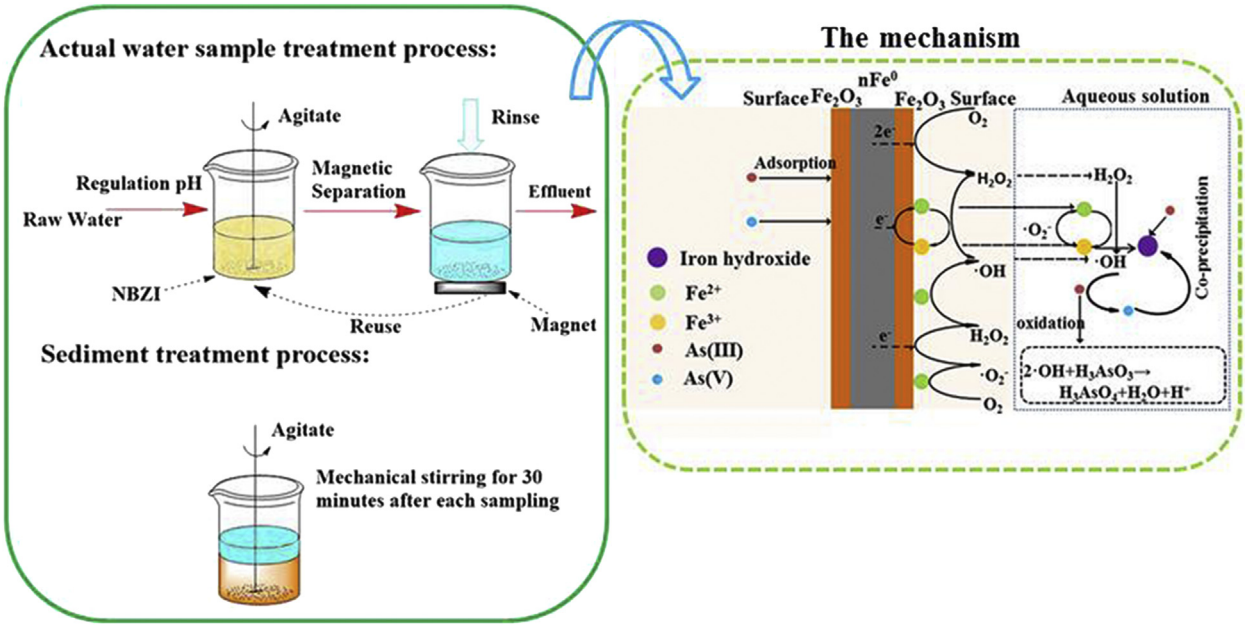

Scheme 1. Possible pathways of anoxic treatment of arsenic by NBZI.

arsenic by adsorption and co-precipitation. Meanwhile, the new Fenton-like system of combing NBZI with H_2O_2 was proposed that could efficiently remove As(III) in anoxic condition due to continuously accelerated Fe^0 corrosion and the improved oxidation capacity. The successful removal of arsenic in acid wastewater and transformation of arsenic speciation in sediment by NBZI provide a promising method to alleviate the arsenic pollution hazards likely posed to the surrounding environment.

Acknowledgements

The study was financially supported by Projects 51579096, 51521006, 51222805, 51508175 and 51409024 supported by National Natural Science Foundation of China, the National Program for Support of Top–Notch Young Professionals of China (2012), and the Program for New Century Excellent Talents in University from the Ministry of Education of China (NCET–11–0129).

Appendix A. Supplementary data

Supplementary data related to this article can be found at http://dx.doi.org/10.1016/j.watres.2017.03.059.

References

Ai, Z., Lu, L., Li, J., Zhang, L., Qiu, J., Wu, M., 2007. Fe@Fe_2O_3 core-shell nanowires as iron reagent. 1. Efficient degradation of rhodamine B by a novel sono-Fenton process. J. Mater. Chem. C 111 (11), 4087–4093.
Ai, Z., Gao, Z., Zhang, L., He, W., Yin, J.J., 2013. Core-shell structure dependent reactivity of Fe@Fe_2O_3 nanowires on aerobic degradation of 4-chlorophenol. Environ. Sci. Technol. 47 (10), 5344–5352.
Appelo, C.A., Mj, V.D.W., Tournassat, C., Charlet, L., 2002. Surface complexation of ferrous iron and carbonate on ferrihydrite and the mobilization of arsenic. Environ. Sci. Technol. 36 (14), 3096–3103.
Baikousi, M., Georgiou, Y., Daikopoulos, C., Bourlinos, A.B., Filip, J., Zboril, R., Deligiannakis, Y., Karakassides, M.A., 2015. Synthesis and characterization of robust zero valent iron/mesoporous carbon composites and their applications in arsenic removal. Carbon 93, 636–647.
Cheng, Z., Fu, F., Dionysiou, D.D., Tang, B., 2016. Adsorption, oxidation, and reduction behavior of arsenic in the removal of aqueous As(III) by mesoporous Fe/Al bimetallic particles. Water Res. 96, 22–31.
De Jonge, M., Teuchies, J., Meire, P., Blust, R., Bervoets, L., 2012. The impact of increased oxygen conditions on metal-contaminated sediments part I: effects on redox status, sediment geochemistry and metal bioavailability. Water Res. 46 (7), 2205–2214.
Du, Y., Fan, H., Wang, L., Wang, J., Wu, J., Dai, H., 2013. á-Fe_2O_3 nanowires deposited diatomite: highly efficient absorbents for the removal of arsenic. J. Mater. Chem. A 26 (26), 7729–7737.
Farrell, J., Wang, J., O'Day, P., Conklin, M., 2001. Electrochemical and spectroscopic study of arsenate removal from water using zero-valent iron media. Environ. Sci. Technol. 35 (10), 2026–2032.
Fonti, V., Beolchini, F., Rocchetti, L., Dell'Anno, A., 2015. Bioremediation of contaminated marine sediments can enhance metal mobility due to changes of bacterial diversity. Water Res. 68, 637–650.
Giasuddin, A.B.M., Kanel, S.R., Choi, H., 2007. Adsorption of humic acid onto nanoscale zerovalent iron and its effect on arsenic removal. Environ. Sci. Technol. 41 (6), 2022–2027.
Gu, Z., Deng, B., Yang, J., 2007. Synthesis and evaluation of iron-containing ordered mesoporous carbon (FeOMC) for arsenic adsorption. Microporous. Mesoporous. Mater. 102 (102), 265–273.
Guan, X., Du, J., Meng, X., Sun, Y., Sun, B., Hu, Q., 2012. Application of titanium dioxide in arsenic removal from water: a review. J. Hazard. Mater 215–216 (10), 1–16.
Guo, X., Zhe, Y., Dong, H., Guan, X., Ren, Q., Lv, X., Xin, J., 2015. Simple combination of oxidants with zero-valent-iron (ZVI) achieved very rapid and highly efficient removal of heavy metals from water. Water Res. 88, 671–680.
Han, X., Song, J., Li, Y.L., Jia, S.Y., Wang, W.H., Huang, F.G., Wu, S.H., 2016. As(III) removal and speciation of Fe (Oxyhydr)oxides during simultaneous oxidation of As(III) and Fe(II). Chemosphere 147, 337–344.
Jang, Min, Soohong, Min, Takhyun Kim, A., Park, J.K., 2006. Removal of arsenite and arsenate using hydrous ferric oxide incorporated into naturally cccurring porous diatomite. Environ. Sci. Technol. 40 (5), 1636–1643.
Kanel, S.R., Manning, B., Charlet, L., Choi, H., 2005. Removal of arsenic(III) from groundwater by nanoscale zero-valent iron. Environ. Sci. Technol. 39 (5), 1291–1298.
Kanel, S.R., Grenèche, J.M., Choi, H., 2006. Arsenic(V) Removal from groundwater using nano scale zero-valent iron as a colloidal reactive barrier material. Environ. Sci. Technol. 40 (6), 2045–2050.
Keenan, C.R., Sedlak, D.L., 2008. Factors affecting the yield of oxidants from the reaction of nanoparticulate zero-valent iron and oxygen. Environ. Sci. Technol. 42 (4), 1262–1267.
Konthur, Z., Nonhoff, U., Wiemkes, M.M., Detert, J., Braun, T., Hollidt, J.M., Burmester, G.R., Skriner, K., 2013. Arsenic removal with composite iron matrix filters in Bangladesh: a field and laboratory study. Environ. Sci. Technol. 47 (9), 4544–4554.
Liu, H., Zuo, K., Vecitis, C., 2014. Titanium dioxide-coated carbon nanotube network filter for rapid and effective arsenic sorption. Environ. Sci. Technol. 48 (23), 13871–13879.
Lu, L., Ai, Z., Li, J., Zheng, Z., Quan, L., Zhang, L., 2007. Synthesis and characterization of Fe–Fe_2O_3 core–shell nanowires and nanonecklaces. Cryst. Growth Des. 7 (2), 459–464.
Lv, X., Xu, J., Jiang, G., Tang, J., Xu, X., 2011. Highly active nanoscale zero-valent iron (nZVI)–Fe_3O_4 nanocomposites for the removal of chromium (VI) from aqueous solutions. J. Colloid Interf. Sci. 369 (1), 460–469.

Manning, B., Hunt, M., Amrhein, C., Yarmoff§, J., 2002. Arsenic (III) and arsenic (V) reactions with zerovalent iron corrosion products. Environ. Sci. Technol. 36 (24), 5455–5461.
Meng, F., Morin, S.A., Jin, S., 2011. Rational solution growth of α-FeOOH nanowires driven by screw dislocations and their conversion to α-Fe_2O_3 nanowires. J. Am. Chem. Soc. 133 (22), 8408–8411.
Neumann, A., Kaegi, R., Voegelin, A., Hussam, A., Munir, A.K., Hug, S.J., 2013. Arsenic removal with composite iron matrix filters in Bangladesh: a field and laboratory study. Environ. Sci. Technol. 47 (9), 4544–4554.
Noubactep, C., 2008. A critical review on ther process of contaminant removal in Fe-HO system. Environ. Technol. 29 (8), 909–920.
Que, L.J., Tolman, W.B., 2008. Biologically inspired oxidation catalysis. Nature 455 (7211), 333–340.
Ramos, M.A.V., Yan, W., Li, X., Koel, B.E., Zhang, W., 2009. Simultaneous oxidation and reduction of arsenic by zero-valent iron nanoparticles: understanding the significance of the core–shell structure. J. Mater. Chem. C 113 (33), 14591–14594.
Salomons, W., 2006. Adsorption of common schemes for single and sequential extractions of trace metal in soils and sediments. Int. J. Environ. An. Ch 51 (51), 3–4.
Shi, J., Ai, Z., Zhang, L., 2014. Fe@Fe_2O_3 core-shell nanowires enhanced Fenton oxidation by accelerating the Fe(III)/Fe(II) cycles. Water Res. 59C (4), 145–153.
Soylak, M., 2015. Characterization of heavy metal fractions in agricultural soils by sequential extraction procedure: the relationship between soil properties and heavy metal fractions. Soil Sediment. Contam. 24 (1), 1–15.
Tang, J., Tang, L., Feng, H., Zeng, G., Dong, H., Zhang, C., Huang, B., Deng, Y., Wang, J., Zhou, Y., 2016. pH-Dependent degradation of p-nitrophenol by sulfidated nanoscale zerovalent iron under aerobic or anoxic conditions. J. Hazard. Mater 320, 581–590.
Tang, L., Zeng, G.M., Shen, G.L., Li, Y.P., Zhang, Y., Huang, D.L., 2008. Rapid detection of picloram in agricultural field samples using a disposable immunomembrane-based electrochemical sensor. Environ. Sci. Technol. 42 (4), 1207–1212.
Tang, L., Tang, J., Zeng, G.M., Yang, G., Xie, X., Zhou, Y., Pang, Y., Fang, Y., Wang, J., Xiong, W., 2015. Rapid reductive degradation of aqueous p-nitrophenol using nanoscale zero-valent iron particles immobilized on mesoporous silica with enhanced antioxidation effect. Appl. Surf. Sci. 333, 220–228.
Tang, L., Yang, G., Zeng, G.M., Cai, Y., Li, S., Zhou, Y., Pang, Y., Liu, Y., Zhang, Y., 2014. Brandon Luna. Synergistic effect of iron doped ordered mesoporous carbon on adsorption-coupled reduction of hexavalent chromium and the relative mechanism study. Chem. Eng. J. 239, 114–122.
Tang, W., Su, Y., Li, Q., Gao, S., Shang, J.K., 2013. Superparamagnetic magnesium ferrite nanoadsorbent for effective arsenic (III, V) removal and easy magnetic separation. Water Res. 47 (11), 3624–3634.
Vadahanambi, S., Lee, S.H., Kim, W.J., Oh, I.K., 2013. Arsenic removal from contaminated water using three-dimensional graphene-carbon nanotube-iron oxide nanostructures. Environ. Sci. Technol. 47 (18), 10510–10517.
Velimirovic, M., Carniato, L., Simons, Q., Schoups, G., Seuntjens, P., Bastiaens, L., 2014. Corrosion rate estimations of microscale zerovalent iron particles via direct hydrogen production measurements. J. Hazard. Mater 270 (3), 18–26.
Wang, C., Luo, H., Zhang, Z., Yan, W., Jian, Z., Chen, S., 2014. Removal of As(III) and As(V) from aqueous solutions using nanoscale zero valent iron-reduced graphite oxide modified composites. J. Hazard. Mater 268C (3), 124–131.
Wen, J., Yi, Y., Zeng, G., 2016. Effects of modified zeolite on the removal and stabilization of heavy metals in contaminated lake sediment using BCR sequential extraction. J. Environ. Manag. 178, 63–69.
Weng, L., Riemsdijk, W.H.V., Koopal, L.K., Hiemstra, T., 2006. Adsorption of humic substances on goethite: comparison between humic acids and fulvic acids. Environ. Sci. Technol. 40 (24), 7494–7500.
Yan, L., Huang, Y., Cui, J., Jing, C., 2015. Simultaneous As(III) and Cd removal from copper smelting wastewater using granular TiO(2) columns. Water Res. 68, 572–579.
Yang, G., Tang, L., Zeng, G., Cai, Y., Tang, J., Pang, Y., Zhou, Y., Liu, Y., Wang, J., Zhang, C., Xiong, W., 2015. Simultaneous removal of lead and phenol contamination from water by nitrogen-functionalized magnetic ordered mesoporous carbon. Chem. Eng. J. 259, 854–864.
Yi, M., Hao, W., Ai, Z., 2015. Negative impact of oxygen molecular activation on Cr(VI) removal with core–shell Fe@Fe_2O_3 nanowires. J. Hazard. Mater 298, 1–10.
Zhang, Y., Zeng, G., Lin, T., Huang, D., Jiang, X., Chen, Y., 2007. A hydroquinone biosensor using modified core–shell magnetic nanoparticles supported on carbon paste electrode. Biosens. Bioelectron. 22 (9–10), 2121–2126.
Zhou, Y., Tang, L., Yang, G., Zeng, G., Deng, Y., Huang, B., Cai, Y., Tang, J., Wang, J., Wu, Y., 2014. Phosphorus–doped ordered mesoporous carbons embedded with Pd/Fe bimetal nanoparticles for the dechlorination of 2,4–dichlorophenol. Catal. Sci. Technol. 6 (6), 1930–1939.
Zhu, H., Jia, Y., Xing, W., He, W., 2009. Removal of arsenic from water by supported nano zero-valent iron on activated carbon. J. Hazard. Mater 172 (2–3), 1591–1596.